Hindawi
Advances in Civil Engineering
Volume 2019, Article ID 8737561, 14 pages
https://doi.org/10.1155/2019/8737561

Research Article

Buckling Analysis of Sandwich Plate Systems with Stiffening Ribs: Theoretical, Numerical, and Experimental Approaches

Guangping Zou,[1] **Yuyang Wang**,[1] **Qichao Xue**,[1,2] **and Chunwei Zhang**[2]

[1]*College of Aerospace and Civil Engineering, Harbin Engineering University, Harbin 150001, China*
[2]*Department of Civil Engineering, Qingdao University of Technology, Qingdao, China*

Correspondence should be addressed to Qichao Xue; xueqichao@hrbeu.edu.cn

Received 21 November 2018; Revised 9 January 2019; Accepted 4 February 2019; Published 4 March 2019

Academic Editor: Chiara Bedon

This paper discusses a global buckling analysis approach for sandwich plates with stiffening ribs. The approach is based on theoretical study and is implemented by the finite element method (FEM). The equilibrium equation corresponding to critical global buckling of the sandwich plate with stiffening ribs under simple supported boundary condition is established by the energy method. The critical buckling solutions for a typical rectangular sandwich plate system (SPS) with a single stiffening rib in the longitudinal direction are then investigated while varying the potential influencing factors. The shear rigidity within the inner core exerts little effect on global buckling and can be neglected. An FEM study on elastic buckling was then conducted via ANSYS software. The advantages of the SPS were highlighted via its elastic eigenvalue buckling numerical analysis with multiple stiffeners. The ultimate buckling loads were computed similarly for different influential factors. Finally, an SPS specimen was tested in a compression test. The results showed that when the rib spacing is large, the local buckling of the plates in the grillage is controllable and the SPS is more resistant to both local and global buckling. The results based on our theoretical method agreed well with those of the FEM and experimental results.

1. Introduction

Steel sandwich panels comprise two solid faceplates and one low-density core. Initially installed in aerospace equipment, they are now increasingly used in shipbuilding. A new type of sandwich plate, called the sandwich plate system (SPS), comprises two metal faceplates sandwiching a continuous polyurethane (PU) elastomer core. SPSs are important for weight reduction, rapid reparation, and impact resistance in bridge engineering [1] and the shipbuilding fields [2]. Figure 1 shows the application of SPS in different fields and differentiates the shapes of the SPS from those of conventional structures.

PU elastomer is significantly viscoelastic with high damping characteristics. Therefore, a PU elastomer core can potentially raise the noise isolation and damping behaviors of the whole SPS structure [3]. In shipbuilding, stiffeners are usually bonded with steel plates or sandwich plates to increase the stiffness of the whole structure under variable loads. SPSs with stiffening ribs have several advantages over conventional steel plates; in particular, they increase the corrosion resistance and reduce the processing cost by diminishing the space requirements of the discrete stiffeners [4].

In recent years, applications and simulations of SPS have been extensively researched. Martin [5] conducted static and fatigue tests of an SPS bridge deck. Chunlei et al. [6] calculated the stress distribution in an orthotropic steel bridge deck that was stiffened by SPSs. The lateral load-distribution characteristics of SPS bridges were delineated via numerical simulations by Harris et al. [7]. Based on the finite element method (FEM), Feng et al. [8] developed a new numerical simulation with shell elements for studying SPS structures. Shang [9] studied the typical failure mode and ultimate strength of an SPS in a model test under combined biaxial compression and lateral pressure. Liu et al. [10] analyzed the crashworthiness of a ship with an SPS hull using FEM software. They demonstrated the superior collision resistance and energy-absorbing capacity of the SPS-incorporated structure over the conventional structure. Zou et al. [11] analyzed the effect of adhesive in an equivalent modelling of SPS.

Rib-stiffened plates are the most common engineering applications of SPSs. As analysis approaches and

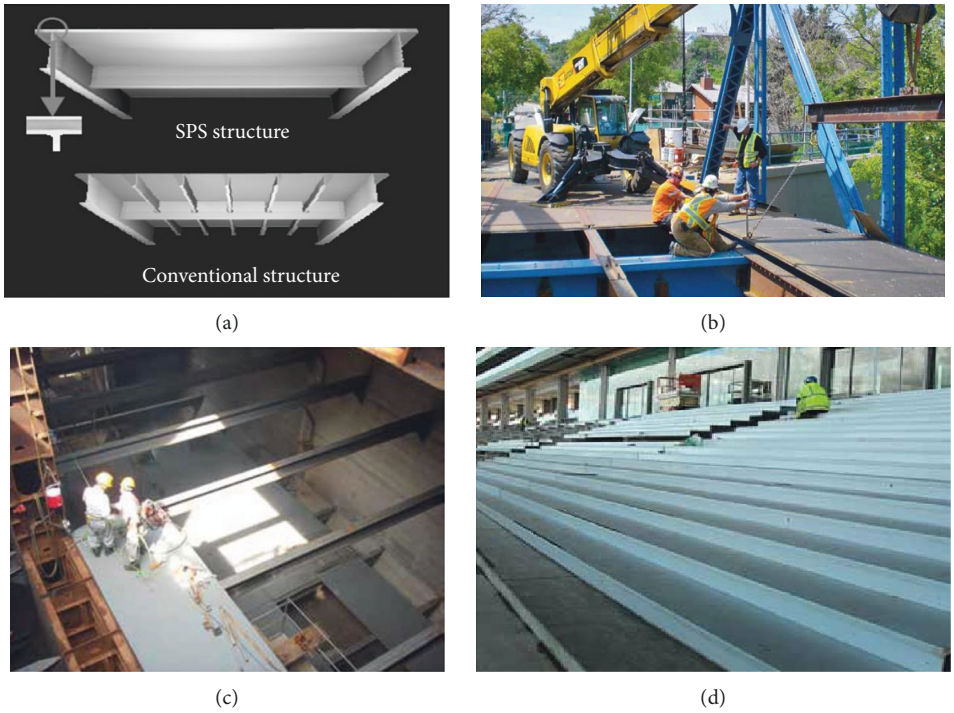

Figure 1: Comparison SPS versus conventional structure: (a) comparison between conventional structure and SPS structure; (b) SPS application as bridge deck; (c) SPS applied as partition board in superstructure of ship; (d) SPS stairs in stadium.

manufacturing techniques of sandwich materials continue to develop, different kinds of sandwich plates are being considered for engineering practice. Two popular examples in the literature are stiffened sandwich plates and plates with viscoelastic properties. Liu and Hollaway [12] presented an optimization procedure for composite panel structures with stiffening ribs under multiple loading cases. Wang and Zhao [13] presented an FEM for vibrating stiffened sandwich plates with moderately thick viscoelastic cores. Gara et al. [14] developed a series of experimental tests and a numerical model for wall sandwich panels. John and Li [15] proposed a new sandwich design with an orthogrid-stiffened syntactic foam core based on shape-memory polymer. Xin and Lu [16] analytically modeled the wave propagation in orthogonally rib-stiffened sandwich structures. Briscoe et al. [17] presented a model of shear buckling and local bearing failure in web-core sandwich panels and validated it in experiments. Goel et al. [18] presented a model and numerical simulation of foam sandwich panels subjected to impulsive loading. Adopting a virtual testing approach, Wadee et al. [19] characterized the mechanical behavior of folded core structures for advanced sandwich composites under flatwise compression loads. Yuan and Dawe [20] numerically analyzed the free vibrations and buckling of sandwich plates using a B-spline finite strip method.

Buckling failure is an important failure mode of plates with stiffening ribs under various conditions. Global buckling of plates with stiffeners was first studied by Timoshenko and Gere [21]. Heder [22] approximated the buckling load of a simply supported stiffened sandwich panel using an energy-based method. Zhao et al. [23] introduced an equivalent laminate modelling method that analyzes the global buckling of stiffened panels with different sectional shapes and stringer distribution forms. Al-Qablan [24] developed a semianalytical buck analysis of stiffened sandwich plates based on first-order shear deformation plate theory (SDPT).

Amadio and Bedon [25–28] studied the effect of variable factors, including multiple mechanical and geometrical aspects, on the buckling behavior of laminated glass elements by combining theoretical methods, numerical simulations, and experiments. In their paper, the normalized resistant domain was proposed for the assessment of the proposed stability check. It was proved that the method was very effective for evaluating buckling behavior of laminated structures through comparing the critical buckling load derived by different analytical interaction formulations. The study was also beneficial to provide us a new theoretical approach to the research of buckling of sandwich panel with ribs.

The present paper theoretically analyzes global buckling in SPSs with stiffening ribs and compares the buckling properties of SPS and conventional rib-stiffened structures. Global buckling is then analyzed via FEM. Finally, an SPS panel stiffened by inner ribs is fabricated and tested in a compression testing facility. Parts of this paper have been published in conference proceedings by the corresponding author [29, 30].

2. Theoretical Buckling Analysis of Sandwich Plates with Stiffening Ribs

2.1. Derivation of Buckling Equation for Ribbed SPSs. SPS is a typical sandwich structure with a PU elastomer core and steel faceplates (Figure 2(a)). The thicknesses of the core and faceplates are denoted by t and t_f, respectively. The system

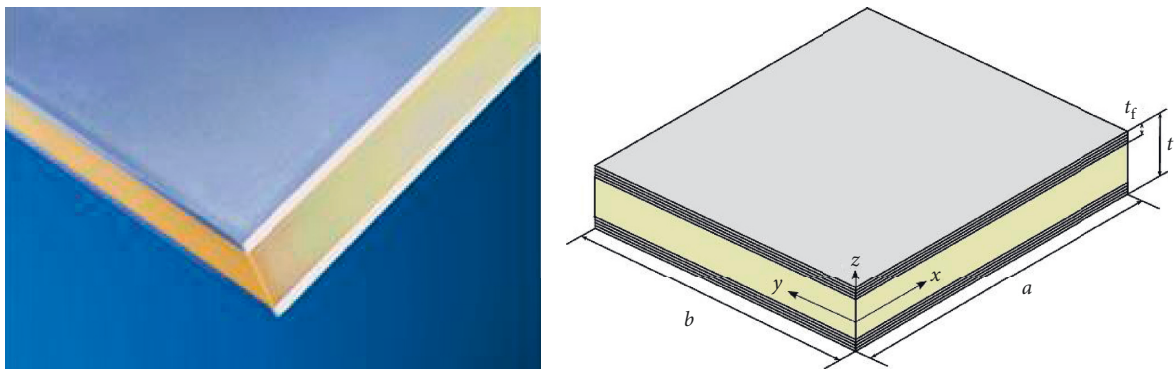

(a) (b)

Figure 2: SPS structure: (a) system sandwich plate system; (b) schematic view of SPS structure.

was set up in Cartesian coordinates with the x-y plane parallel to the in-plane of the sandwich plate, and the z-axis perpendicular to the plane (Figure 2(b)). In engineering practice, SPSs are usually stiffened by ribs inside the core as well as on the cross wall (Figure 3(a)) and plate exterior (Figure 1(a)).

The global theoretical buckling analysis for sandwich plates with stiffener ribs can be combined with the bending theory of sandwich plates and conventional stiffened plates. The analysis was simplified by the following assumptions:

(1) The sandwich plate is modeled by traditional SDPT sandwich plate theory (Hoff's theory), in which only the core bears shear effects under transverse loads. The bending rigidity of the faceplates is also considered.

(2) The SPS stiffeners are perfectly connected with the sandwich plate, and they deform along with the plate at all times. The torsional effect of the stiffeners during buckling is ignored when calculating the critical buckling loads.

As shown in Figure 3, the sandwich plate with rectangular stiffening ribs experiences in-plane pressure under the simply supported boundary conditions. The buckling shape of the global stiffened sandwich plate was expressed as the following bitrigonometric series:

$$w = \sum_{m=1}^{\infty}\sum_{n=1}^{\infty} a_{mn} \sin\frac{m\pi x}{a} \sin\frac{n\pi y}{b}, \tag{1}$$

where w is the out-of-plane deflection function and a and b are the plate length and width, respectively. a_{mn} are the polynomial parameters of the bitrigonometric series, where m is the number of semiwaves and n is the number of ribs. Ignoring the bending stiffness of the core (justified under the above assumptions), the total deformation energy of the global sandwich structure was divided into two parts: the bending deformation energy of the faceplates and the shear deformation energy of the PU elastomer core. The total energy is thus calculated as

$$\Delta U = \Delta U_{\mathrm{bf}} + \Delta U_{\mathrm{tc}}, \tag{2}$$

where ΔU_{bf} and ΔU_{tc} are the bending and shearing deformation energy of the sandwich plate, respectively. Based on traditional sandwich plate theory, the deformation of the sandwich plate was considered as the deformation of a homogeneous plate with the same bending stiffness under external loads plus the shear deformation of the core:

$$w = w_0 - \frac{D_{\mathrm{h}}}{C}\nabla^2 w, \tag{3}$$

where $C = G_{\mathrm{c}}(h + t)$ and G_{c} is the torsional modulus of the core; D_{h} is the equivalent stiffness of the whole Sandwich plate; and w_0 denotes the deformation corresponding to the bending effect, which is similar (in form) to the whole deformation of the sandwich plate:

$$w_0 = \sum_{m=1}^{\infty}\sum_{n=1}^{\infty} b_{mn} \sin\frac{m\pi x}{a} \sin\frac{n\pi y}{b}. \tag{4}$$

Substituting equations (1) and (4) into equation (3), the relation between a_{mn} and b_{mn} is given as

$$b_{mn} = a_{mn}\left(1 - \frac{D_{\mathrm{h}}}{C}\left(\frac{m^2}{a^2} + \frac{n^2}{b^2}\right)\pi^2\right). \tag{5}$$

Setting the parameter $B_{mn} = (1 - (D_{\mathrm{h}}/C)((m^2/a^2) + (n^2/b^2))\pi^2)$, the bending deformation energy becomes

$$\Delta U_{\mathrm{bf}} = \frac{\pi^4 D_{\mathrm{h}}}{2}\frac{ab}{4}\sum_{m=1}^{\infty}\sum_{n=1}^{\infty} B_{mn}^2 a_{mn}^2 \left(\frac{m^2}{a^2} + \frac{n^2}{b^2}\right)^2, \tag{6}$$

where D_{h} defines the bending stiffness of a single face of the panel. Similarly, the bending deformation energy of core was determined as

$$\Delta U_{\mathrm{bc}} = \frac{\pi^4 D_{\mathrm{c}}}{2}\frac{ab}{4}\sum_{m=1}^{\infty}\sum_{n=1}^{\infty} B_{mn}^2 a_{mn}^2 \left(\frac{m^2}{a^2} + \frac{n^2}{b^2}\right)^2, \tag{7}$$

where D_{c} is the bending stiffness of the core. These quantities are, respectively, calculated as follows:

$$D_{\mathrm{h}} = D_0 + 2D_{\mathrm{f}} = \frac{E_{\mathrm{f}}(h + t)^2 t}{2\left(1 - v_{\mathrm{f}}^2\right)} + 2\frac{E_{\mathrm{f}} t^3}{12\left(1 - v_{\mathrm{f}}^2\right)}, \tag{8}$$

where D_0 is the bending stiffness of the whole sandwich plate (ignoring the stiffness of the faceplates). ΔU_{tc} is expressed as

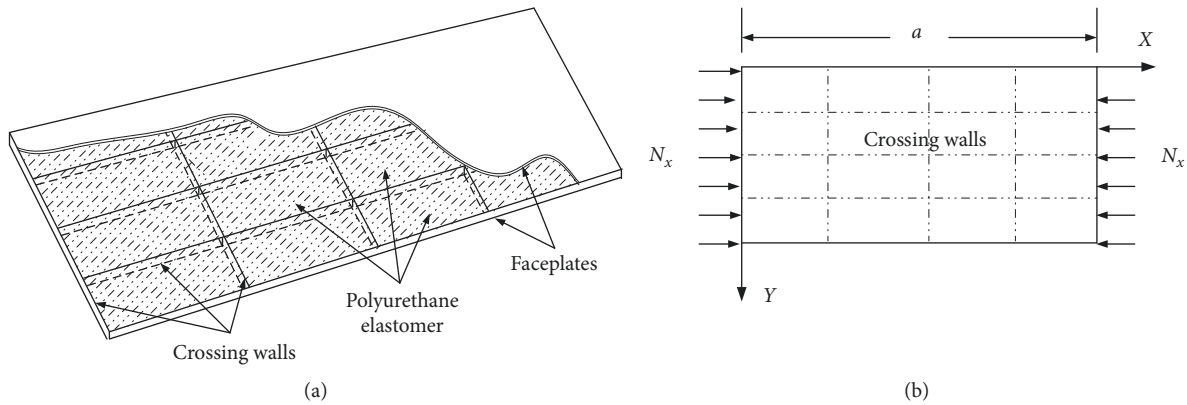

Figure 3: Section of sandwich plate and SPS with stiffeners. (a) Structure sketch of SPS reinforced by cross wall. (b) Simplified loading schematic diagram.

$$\Delta U_{\mathrm{tc}} = \frac{1}{2}\iint_s \left(\tau_{xz}\gamma_{xz} + \tau_{yz}\gamma_{yz}\right)dx\,dy = \frac{h+t}{2G_{\mathrm{c}}}\iint_s \left(\tau_{xz}^2 + \tau_{yz}^2\right)dx\,dy. \tag{9}$$

Under the assumptions of Hoff's plate theory, shear stress is uniformly distributed along the core section. Following the arguments in [31], the shear stress is calculated as

$$\tau_{xz} = \frac{Q_{\mathrm{cx}}}{h+t}, \qquad \tau_{yz} = \frac{Q_{\mathrm{cy}}}{h+t}. \tag{10}$$

The external shear loads Q_{cx} and Q_{cy} are assumed to be uniformly distributed along the section. Using the equilibrium equation of thin-plate bending theory, they are, respectively, expressed as follows:

$$Q_{\mathrm{cx}} = Q_{\mathrm{xh}} - Q_{\mathrm{xf}} = -D_{\mathrm{h}}\frac{\partial}{\partial x}\nabla^2 w + 2D_{\mathrm{f}}\frac{\partial}{\partial x}\nabla^2 w,$$
$$Q_{\mathrm{cy}} = Q_{\mathrm{yh}} - Q_{\mathrm{yf}} = -D_{\mathrm{h}}\frac{\partial}{\partial y}\nabla^2 w + 2D_{\mathrm{f}}\frac{\partial}{\partial y}\nabla^2 w, \tag{11}$$

where E_{f} and v_{f} are Young's modulus and Poisson's ratio of the faceplates, respectively. The subscript c, f, and h represent the core, faceplates, and the whole sandwich plate, respectively. Substituting equations (10) and (11) into equation (9) gives

$$\Delta U_{\mathrm{c}} = \frac{D_0^2}{(h+t)^2}\frac{ab\pi^6}{8G_{\mathrm{c}}}\sum_{m=1}^{\infty}\sum_{n=1}^{\infty} a_{mn}^2\left(\frac{m^2}{a^2} + \frac{n^2}{b^2}\right)^3. \tag{12}$$

As the stiffeners are bonded to the structure, the ribs deform along with the plate; thus, the bending deformation energy ΔU_i is given by

$$\Delta U_i = \frac{\mathrm{EI}_i}{2}\int_0^a \left(\frac{\partial^2 w}{\partial x^2}\right)_{y=c_i}^2 dx = \frac{\pi^4 \mathrm{EI}_i}{4a^3}\sum_{m=1}^{\infty} m^4\left(a_{m_1}\sin\frac{\pi c_i}{b} + a_{m_2}\sin\frac{2\pi c_i}{b} + \cdots\right)^2, \tag{13}$$

where EI_i is the bending stiffness of the rib at distance c_i from the side of the panel ($y = 0$).

When the sandwich panel is buckling, the work ΔT done by the in-plane pressure N_x is given by

$$\Delta T = \frac{N_x}{2}\frac{ab}{4}\sum_{m=1}^{\infty}\sum_{n=1}^{\infty}\frac{m^2\pi^2}{a^2}a_{mn}^2, \tag{14}$$

and the work done by the force P_i acting on each rib is

$$\Delta T_i = \frac{P_i}{2}\int_0^a \left(\frac{\partial w}{\partial x}\right)_{y=c_i}^2 dx\Delta U_{\mathrm{bf}} = \frac{\pi^4 D_h}{2}\frac{ab}{4}\sum_{m=1}^{\infty}\sum_{n=1}^{\infty} B_{mn}^2 a_{mn}^2\left(\frac{m^2}{a^2} + \frac{n^2}{b^2}\right)^2 = \frac{\pi^2 P_i}{4a}\sum_{m=1}^{\infty} m^2\left(a_{m_1}\sin\frac{\pi c_i}{b} + a_{m_2}\sin\frac{2\pi c_i}{b} + \cdots\right)^2. \tag{15}$$

Neglecting the torsional deformation energy of the ribs, the total potential energy is computed as

$$\prod = \Delta U_{\mathrm{bf}} + \Delta U_{\mathrm{bc}} + \Delta U_{\mathrm{tc}} + \Delta\sum_i U_i - \left(\Delta T + \Delta\sum_i T_i\right), \tag{16}$$

adopting the following symbols:

$$\beta = \frac{a}{b}, \qquad \frac{\mathrm{EI}_i}{bD_{\mathrm{h}}} = \gamma_i, \qquad \frac{P_i}{bN_x} = \frac{A_i}{b(h+2t)} = \delta_i, \qquad \sigma_{\mathrm{cr}} = \frac{N_x}{A}, \tag{17}$$

where A_i is the section area of the rib. Substituting equations (12)–(15) and equation (17) into equation (16), the total potential energy becomes

$$\prod = \frac{(D_h + D_c)\sum_{m=1}^{\infty}\sum_{n=1}^{\infty} B_{mn}^2 a_{mn}^2 \left(m^2 + n^2\beta^2\right)^2 + \left(\pi^2 D_0^2 / G_c (h+t)^2\right)\sum_{n=1}^{\infty} a_{mn}^2 \left(m^2 + n^2\beta^2\right)^3}{\sum_{m=1}^{\infty}\sum_{n=1}^{\infty} a_{mn}^2 m^2 + 2\sum_i \delta_i \sum_{m=1}^{\infty} m^2 \left(\sum_{n=1}^{\infty} a_{mn} \sin\left(n\pi c_i / b\right)\right)^2} + \frac{2\sum_i D_h \gamma_i \sum_{m=1}^{\infty} m^4 \left(\sum_{n=1}^{\infty} a_{mn} \sin\left(n\pi c_i / b\right)\right)}{\sum_{m=1}^{\infty}\sum_{n=1}^{\infty} a_{mn}^2 m^2 + 2\sum_i \delta_i \sum_{m=1}^{\infty} m^2 \left(\sum_{n=1}^{\infty} a_{mn} \sin\left(n\pi c_i / b\right)\right)^2} - \frac{b^2 (h+2t)\beta^2}{\pi^2}\sigma_{cr}. \tag{18}$$

Equating Π to 0 in equation (18), we obtain

$$\begin{aligned} 0 = {} & \frac{\pi^2}{b^2\beta^2 (h+2t)} \times \left[(D_h + D_c) \sum_{m=1}^{\infty}\sum_{n=1}^{\infty} B_{mn}^2 a_{mn}^2 \left(m^2 + n^2\beta^2\right)^2 \right. \\ & + \frac{\pi^2 D_0^2}{b^2\beta^2 G_c (h+t)} \sum_{m=1}^{\infty}\sum_{n=1}^{\infty} a_{mn}^2 \left(m^2 + n^2\beta^2\right)^3 \\ & \left. + 2\sum_i D_h \gamma_i \sin\frac{n\pi c_i}{b} m^4 \left(\sum_{p=1}^{\infty} a_{mp} \sin\frac{p\pi c_i}{b} \right) \right] \\ & - \sigma_{cr} \left[a_{mn} m^2 + 2\sum_i \delta_i \sin\frac{n\pi c_i}{b} m^2 \left(\sum_{p=1}^{\infty} a_{mp} \sin\frac{p\pi c_i}{b} \right) \right]. \end{aligned} \tag{19}$$

Equation (18) computes the critical buckling load for different numbers of ribs.

2.2. Global Buckling Calculation for a Sandwich Plate with One Rib. To verify the effectiveness of previous analyses and investigate the differences between sandwich plates and conventional stiffening plates, we first explored the influences of various parameters on a single-ribbed sandwich plate. As shown in Figure 4, the sandwich plate is arranged with only one rib in the center of the plate, and the width of the plate is divided into equal intervals, meaning that c_i equaled to $b/2$. Assuming one buckling wave along the y-axis (i.e., $n = 1$) and half a wave along the x-axis (i.e., $m = 1$) as a typical example, equation (18) can be written as follows:

$$\begin{aligned} 0 = {} & \frac{\pi^2}{b^2\beta^2 (h+2t)} \left[(D_h + D_c) a_1 B_{mn}^2 \left(1+\beta^2\right)^2 \right. \\ & \left. + \frac{\pi^2 D_0^2}{G_c\beta^2 b^2 (h+t)} a_1 \left(1+\beta^2\right)^3 \right] + \left[\frac{2\pi^2 D_h \gamma}{b^2\beta^2 (h+2t)} - 2\delta\sigma_{cr} \right] \\ & \cdot \left(a_1 - a_3 + a_5 - \cdots\right) - a_1\sigma_{cr}, \\ 0 = {} & \frac{\pi^2}{b^2\beta^2 (h+2t)} \left[(D_h + D_c) a_2 B_{mn}^2 \left(1+4\beta^2\right)^2 \right. \\ & \left. + \frac{\pi^2 D_0^2}{G_c\beta^2 b^2 (h+t)} a_2 \left(1+4\beta^2\right)^3 \right] - a_2\sigma_{cr}, \\ 0 = {} & \frac{\pi^2}{b^2\beta^2 (h+2t)} \left[(D_h + D_c) a_3 B_{mn}^2 \left(1+9\beta^2\right)^2 \right. \\ & \left. + \frac{\pi^2 D_0^2}{G_c\beta^2 b^2 (h+t)} a_3 \left(1+9\beta^2\right)^3 \right] + \left[\frac{2\pi^2 D_h \gamma}{b^2\beta^2 (h+2t)} + 2\delta\sigma_{cr} \right] \\ & \cdot \left(a_1 - a_3 + a_5 - \cdots\right) - a_3\sigma_{cr}, \\ 0 = {} & \frac{\pi^2}{b^2\beta^2 (h+2t)} \left[(D_h + D_c) a_2 B_{mn}^2 \left(1+16\beta^2\right)^2 \right. \\ & \left. + \frac{\pi^2 D_0^2}{G_c\beta^2 b^2 (h+t)} a_2 \left(1+16\beta^2\right)^3 \right] - a_4\sigma_{cr} \cdots \end{aligned} \tag{20}$$

In thin-plate bending theory with stiffeners, the first-order critical buckling loads are approximated by equation (20). All terms a_{mn} are equaled to 0 except a_1, the first term of the double triangular series. Introducing the parameter φ,

$$\varphi = \frac{\pi^2 D_0^2}{G_c\beta^2 b^2 D_h (h+t)^2} \left(1+\beta^2\right)^3, \tag{21}$$

σ_{cr} can be written as

$$\sigma_{cr} = \frac{\pi^2 D_h}{b^2 (h+2t)} \frac{B_{mn}^2 \left(1+\beta^2\right)^2 + \varphi + 2\gamma}{\beta^2 (1+2\delta)}. \tag{22}$$

The parameter φ relates to the shear deformation work done by the core. Introducing the coefficient of critical buckling k,

$$k = \frac{B_{mn}^2 \left(1+\beta^2\right)^2 + \varphi + 2\gamma}{\beta^2 (1+2\delta)}, \tag{23}$$

σ_{cr} finally becomes

$$\sigma_{cr} = k \frac{\pi^2 D_h}{b^2 (h+2t)}. \tag{24}$$

When n is even, the parameter a_{mn} in equation (20) takes a single value, and equation (20) expresses the deflection of the internode line. When the sandwich panel is uniformly buckled to generate an even number of semiwaves along the y direction, the internode line remains straight, meaning that the ribs arranged along the center of the plate are nonfunctional.

As β increases, multiple semiwaves may appear in the compression loading direction ($m \neq 1$). Therefore, substituting m in equation (20), we obtained the total potential energy. The potential energy of a sandwich plate with n ribs is calculated by substituting $c_i = b/(n+1)$ in equation (19). The first-order critical buckling loads are approximately given by

$$\sigma_{cr} = \frac{\pi^2 D_h}{b^2 (h+2t)} \frac{B_{mn}^2 \left(1+\beta^2\right)^2 + \varphi + 2\sum_i \gamma_i \sin^2\left(\pi c_i / b\right)}{\beta^2 \left(1 + 2\sum_i \delta_i \sin^2\left(\pi c_i / b\right)\right)}. \tag{25}$$

2.3. Examples of Solutions to Buckling Theory. Stiffeners influence sandwich plates with single and multiple ribs in a similar manner. Therefore, as an example, we analyzed a simple supported rectangular sandwich panel with a single rib (Figure 4). The length b is 2030 mm, and the width a is calculated from β. The faceplate and core thicknesses are $t = 2$ mm and $h = 13.6$ mm, respectively. For steel faceplates,

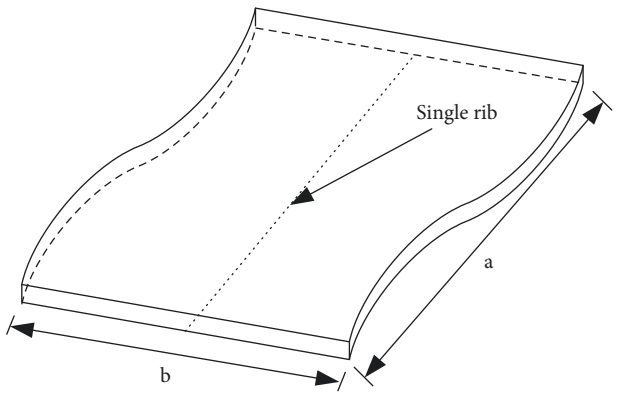

Figure 4: Straight rib when the plate is buckling.

Young's modulus is $E = 2.1 \times 10^5$ MPa and Poisson's ratio is 0.3. The shear modulus G_c of the core is taken as 308 MPa.

According to equation (22), the critical stress is governed by the bending stiffness of the components in the sandwich plates. The critical stresses for different stiffness (equation (8)) in the above example are listed in Table 1.

As shown in Table 1, the total bending stiffness of the sandwich plate is 0.55% higher when considering the bending stiffness of the faceplate than when not considering the stiffness factor. Moreover, the bending stiffness of the core is approximately 0.32% of the overall bending of the bending rigidity of the sandwich plate. Therefore, we concluded that the bending stiffness of the faceplates can be ignored when calculating the bending stiffness.

In engineering practice, the cross-sectional area of the ribs is 2%–10% of the section area of the plates. In the present example, the stiffener is considered to cover 5% of the cross-sectional area of the plate. The effect of the inertia moment of the stiffening rib is then investigated under critical buckling loads.

When the faceplate thickness is fixed, increasing the core thickness will increase the bending stiffness of the whole structure. Figure 5 plots the effect of core thickness on the critical buckling load for different β. The faceplate thickness and inertia moment are fixed at 2 mm and (418×10^4) mm^4, respectively. Increasing the core thickness increased the bending stiffness of the SPS. Here, we considered only the first buckling semiwave. Lowering the β value reduced the influence of the core thickness: at low β, the corresponding curve changed gently; at higher β, it increased more sharply.

Figure 6 shows the critical buckling loads in the case of multiple semiwave buckling, corresponding to different core thicknesses. The inertia moment of the rib is fixed at 418×10^4 mm^4.

As shown in Figure 6, the critical buckling load changed slowly with the thickness of the core in sandwich plates. Increasing the core thickness from 5 to 50 mm significantly increased the critical buckling load from approximately 5000 N/mm to 11000 N/mm. This result can be explained by the sharp increase in bending stiffness of the SPS as the core thickness increased.

Figure 7 relates the critical buckling coefficient to the inertia moment of the rib for different numbers of semiwaves, where the section area of the ribs is 2% of the total section area. The critical buckling coefficient is quite sensitive to the inertia moment of the stiffening ribs. When the bending stiffness of the ribs is ignored, the critical coefficient is minimized when the SPS panel buckled into two semiwaves ($n = 1$, $m = 2$); as the bending stiffness of the ribs increased above 81.7 cm^4, the critical coefficient appeared at

Table 1: Different rigidities of the sandwich plate.

Bending stiffness	D_0	D_f	D_h	D_c
Value	56.162 N/mm	0.153 N/mm	56.474 N/mm	0.184 N/mm

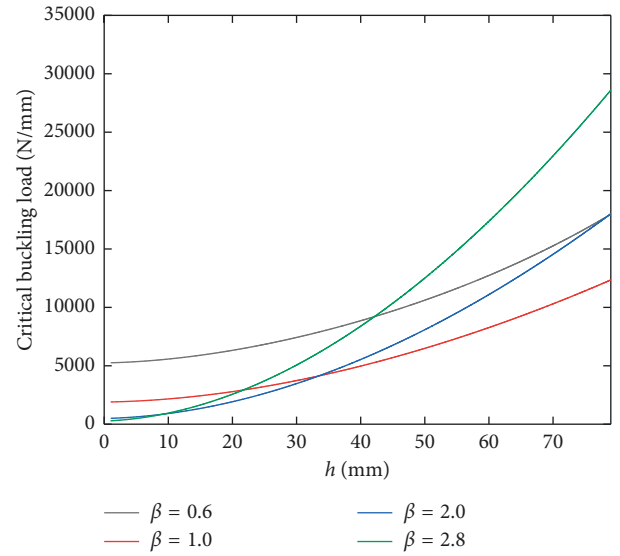

Figure 5: Relation between critical buckling load and core thickness for different β.

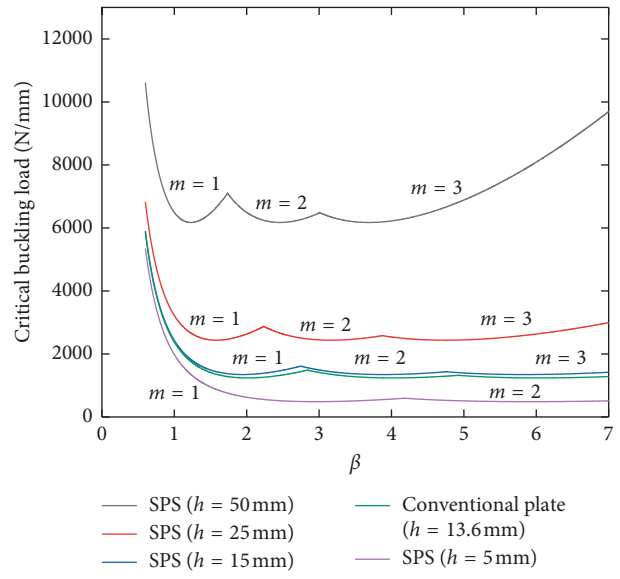

Figure 6: Relation between critical buckling load and β for different core thicknesses.

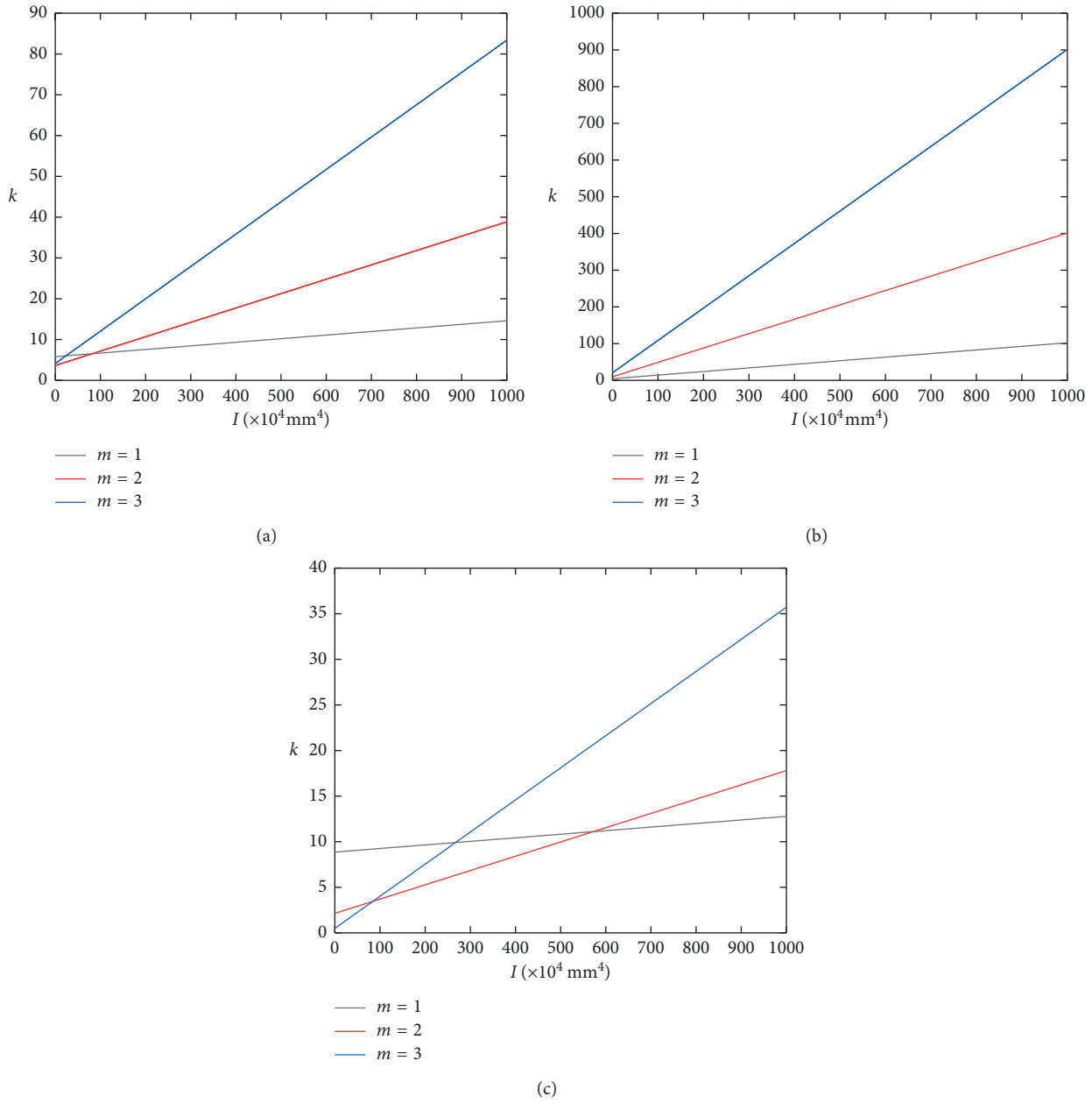

Figure 7: Relation between critical buckling load coefficient k and rib inertia moment for (a) $\beta = 2$, (b) $\beta = 0.6$, and (c) $\beta = 3$.

lower values in the curve with the hollow circles. This result indicates a change in the buckling of the SPS structure from two semiwaves to one semiwave ($m = 1$) along the x direction.

As the three curves in Figure 7(b) do not intersect, changing the inertia moment of the stiffening rib did not affect the buckling wave number, and the corresponding buckling waveform remained as one semiwave. As seen in Figure 7(c), when the stiffening rib is not installed on the sandwich panel, the buckling waveform is three half-waves. For small inertia moments of the stiffening rib, the buckling form exhibited two semiwaves. As the inertia moment of the stiffening rib increased, the sandwich panel buckled into one semiwave, indicating a major role of the stiffening rib in the buckling of the overall structure. The critical buckling stress in a conventional plate with ribs is given by

$$\sigma_{cr} = \frac{\pi^2 D_h}{b^2 (h + 2t)} \frac{D_h B_{mn}^2 \left(1 + \beta^2\right)^2 + \varphi + 2\gamma}{\beta^2 (1 + 2\delta)}. \tag{26}$$

The β values at the critical buckling load for different inertia moments of a single rib on the SPS and steel plates are displayed in Figure 8. According to these curve, the inertia moment significantly affects the critical buckling load. A low critical buckling load always accompanies a small inertia moment but cannot fall below the critical buckling load of the structure without the rib. The critical buckling load tended to increase with increasing inertia moment of the

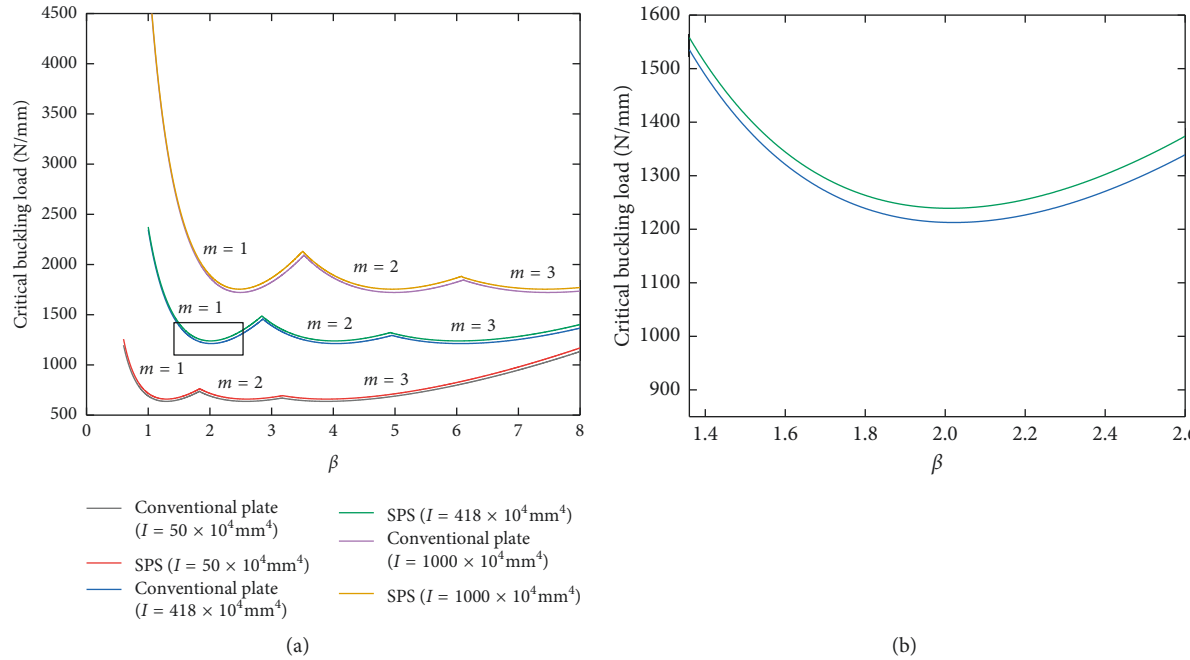

Figure 8: Relation between β and critical buckling load for different inertia moments of a single rib on the SPS and steel plates. (a) Original relations between β and critical buckling loads. (b) Local enlargement of the curves in (a).

ribs, but the growth trend of critical buckling stress gradually slows down. Meanwhile, the inertia moment is positively correlated with the buckling wavelength.

Clearly, when the inertia moment of the rib is small, the critical buckling load is also small but is lower-limited by the load without the ribs. After decreasing by a certain degree, the load grew slowly with increasing inertia moment. Increasing the inertia moment also increased the buckling wavelength.

Figure 8(b) in a zoom-in of the area delineated by the rectangular frame in Figure 8(a). The upper and lower curves are the results of SPS considering the shearing deformation energy and the equivalent conventional steel structure, respectively. The small gap between the two curves implies that the shearing deformation energy can be neglected.

Figure 9 plots the critical buckling stresses as functions of β for different inertia moments of a single rib on the SPS and conventional steel plate. The critical buckling stress significantly differed between the two curves. Moreover, the absolute value of this difference increased roughly proportionally to the critical buckling stress. The reasons are explained as follows: as the critical buckling loads are similar for the SPS and conventional plates, the larger cross-sectional area of the sandwich plates in comparison with the conventional plates reduces the critical stress in the former relative to the latter. The ratio of the critical buckling stresses in the sandwich and homogeneous plates is computed from equations (24) and (26) as

$$B_{mn}\frac{h_0}{h+2t} = B_{mn}\frac{\sqrt[3]{12\left(\left((h+t)^2t\right)/2\right)+\left(t^3/6\right)}}{h+2t}. \quad (27)$$

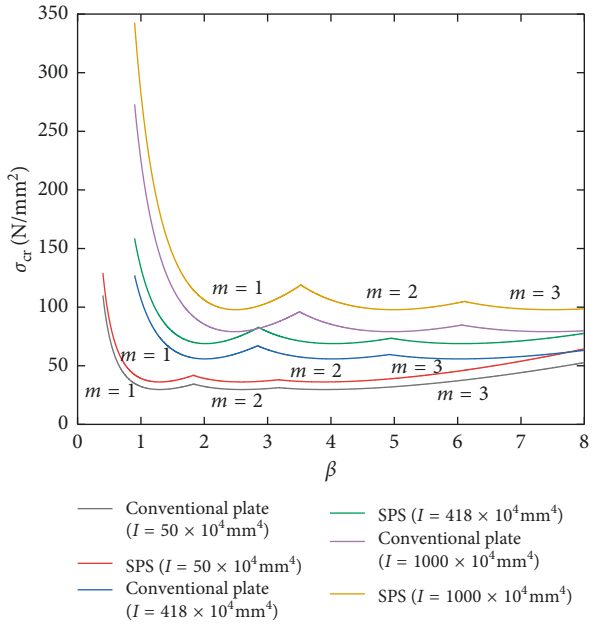

Figure 9: Relation between β and critical buckling stress for different inertia moments of a single rib in the SPS and steel plate.

With their large Young's modulus, the faceplates in the sandwich structure are the main load-bearing components under in-plane compression stress. For the same compression load and cross-sectional area, the compressive stress under a critical buckling load will be higher in the faceplates of SPS than in a conventional steel plate because the faceplates take most of compression load in SPS. The multiplication factor is $(1 + (h/2t))$. At this time, the ratio of the critical buckling stresses in the sandwich and homogeneous plates is given by

$$B_{mn}\frac{h_0}{2t} = B_{mn}\frac{\sqrt[3]{12\left(12\left(\left(\left((h+t)^2 t\right)/2\right) + \left(t^3/6\right)\right)\right)}}{2t}. \quad (28)$$

Figure 10 relates the critical buckling stress to β for different inertia moments of the SPS and steel plates. The critical buckling load under in-plane pressure, at which buckling first appears, is larger in the SPS than in the conventional plate, implying higher internal stresses in the SPS than in the conventional plate.

In typical applications, the ratio δ of the faceplate thickness to the core thickness lied between 1 : 5 and 1 : 10. Substituting δ in equation (28), the ratio of the critical buckling loads of the faceplate and core ranges from 3 to 4.5. For the common beam-plate composite structures in engineering practice, the stress in the plate component is far from the yield strength when overall buckling occurs. Therefore, when the steel plate is made into a sandwich structure, buckling occurs under large inner stress, which improves the utilization of the material.

3. FEM Analyses of SPS and Conventional Plates with Stiffening Ribs

3.1. FEM Eigenvalue Buckling Analysis. The calculations in Section 2 cannot determine the local buckling in SPSs. The critical buckling stress in ribbed sandwich plates is sometimes controlled by local buckling in a single grid. FEM analysis can estimate both the global and local buckling in SPSs and can assess the influences of different factors on the critical buckling loads of conventional plates and SPSs with stiffening ribs.

In this analysis, the material properties are unchanged from those in Section 2, and the stiffening ribs are simulated as beam elements. The conventional steel plates and SPSs are constructed from shell elements. Figure 11 shows the FEM model with $\beta = 2$ and $\beta = 5$.

3.2. Analysis of SPS with a Single Stiffened Rib. To verify the accuracy of the above analysis, the above theoretical calculations are compared with the FEM results of an eigenvalue analysis. The theoretical and FEM results of an SPS with a single stiffening rib for different β values and inertia moments are shown in Figure 12. Here, the inertia moment of the single rib is varied from 5×10^4 to 1000×10^4 mm^4, and β is set to 1.0 (critical buckling load ~450–3000 N/mm) and 2.0 (critical buckling load ~450–1500 N/mm).

The results of both methods are highly consistent and exhibited the same general trends. At some points, the difference between the results is increased by local buckling in certain grids. The error is larger for $\beta < 2$, reflecting the higher inertia of the stiffener rib in this case. When global buckling occurred, the calculation and numerical results are relatively close.

3.3. Result Comparisons for Steel Grillage and SPS with Stiffening Ribs. This subsection first investigates the influence of β on the critical buckling load. In the FEM, the conventional plate is 2000 mm wide and 4 mm thick. Meanwhile, the core and faceplate thicknesses of the SPS are set to 16 mm and 2 mm, respectively. The sandwich panel is stiffened by four ribs with rectangular cross sections. The inertia moment of each rib is 22500 mm^4.

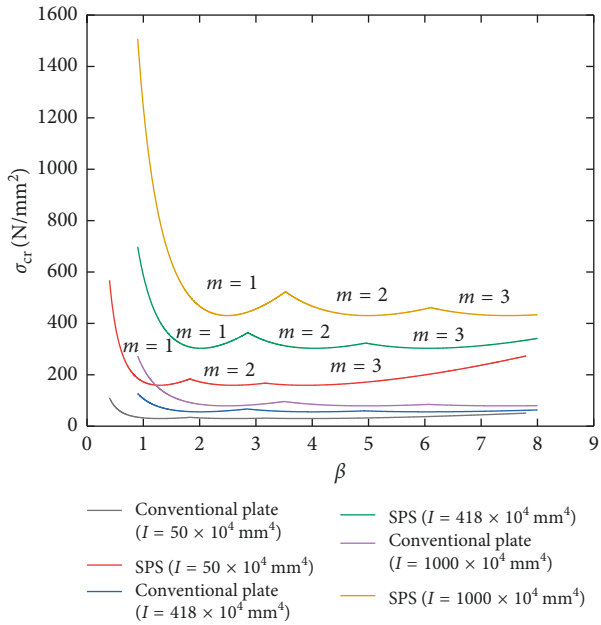

Figure 10: Relation between β and critical buckling stresses (actual) for different inertia moments of the single rib in the SPS and steel plates.

The critical buckling loads for the different β values are shown in Figure 13. The critical buckling loads are approximately three times higher in the ribbed SPS than in the conventional plates, confirming that the core in SPS enhances the bending stiffness of the whole structure. The small bump in both curves indicated a transformation of the buckling shape from one half-wave to two half-waves.

Figure 14 plots the critical buckling load versus inertia moment of the ribs. The critical buckling load is an approximately linear function of number of ribs. However, in the conventional plates, the critical buckling loads tended to remain steady after the inertia moment of the ribs reached a certain threshold. At this time, first-order buckling is not global buckling but in fact local buckling in a single cell of the grillage. Therefore, when the number of ribs in the plates is fixed, enlarging the stiffeners can significantly improve the stability until the appearance of local buckling in one cell of the grillage.

Figure 15 plots the critical buckling loads in the x and y directions in conventional and SPS plates with different numbers of ribs. For a given number of stiffeners, the critical buckling loads are larger in the x direction than in the y direction because the compressive loads are applied in the x direction. Moreover, the critical buckling load along the y direction (Figure 15(b)) increased slightly more rapidly with rib number than the critical buckling load along the x direction (Figure 15(a)), implying that transverse stiffeners exert little influence on the critical buckling loads. Finally,

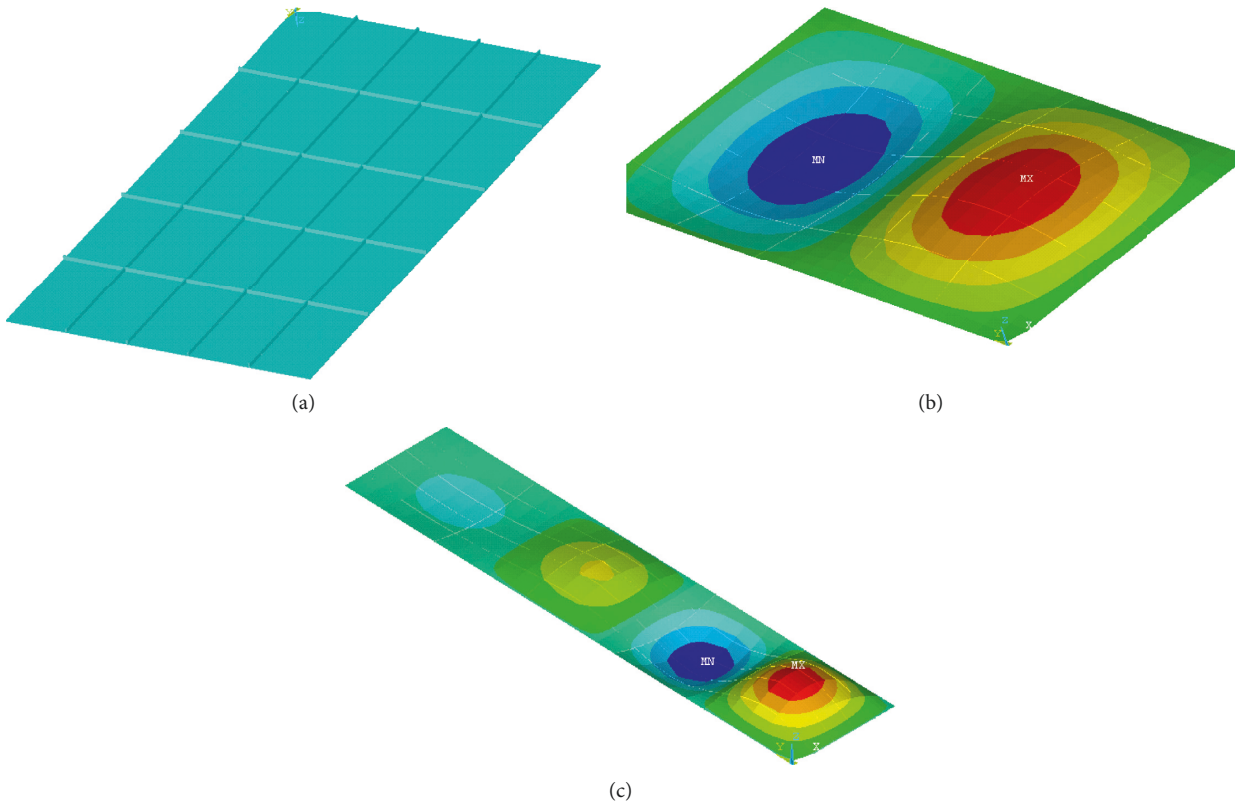

Figure 11: Finite element analysis of plates with stiffeners and the first-order buckling model: (a) ribbed SPS structure in the FEM model, (b) FEM model with $\beta = 2$, and (c) FEM model with $\beta = 5$.

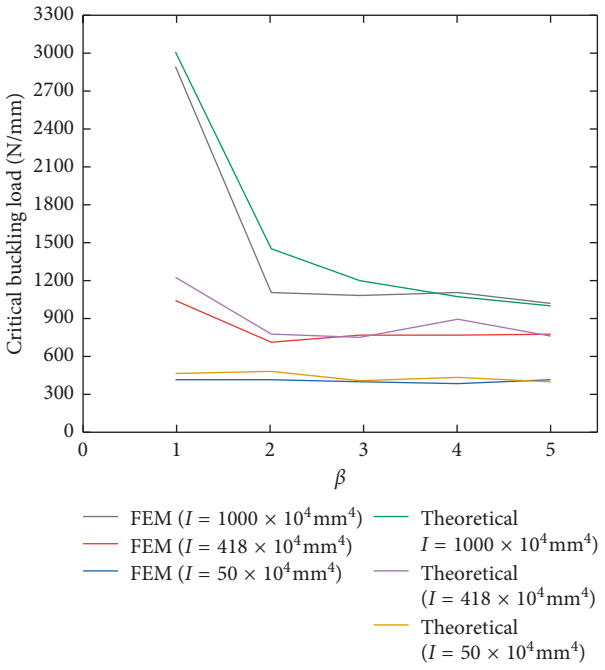

Figure 12: Comparisons between theoretical and FEM results.

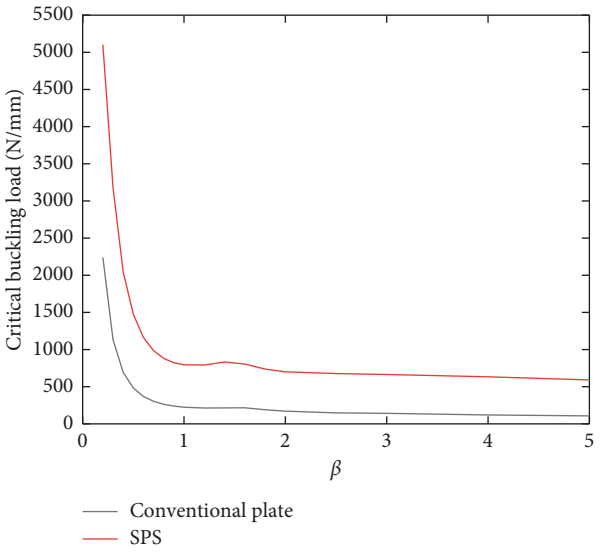

Figure 13: Critical buckling loads in ribbed SPS and conventional plates with different length-to-width ratios.

the SPS structure can withstand higher critical buckling loads than conventional plates with the same number of stiffeners.

4. Buckling Experiment for SPS with Stiffening Ribs

4.1. Design and Preparation of the Test Specimen. To verify the calculation result, a typical SPS model test is conducted in a compression testing machine. The shape and sizes of the

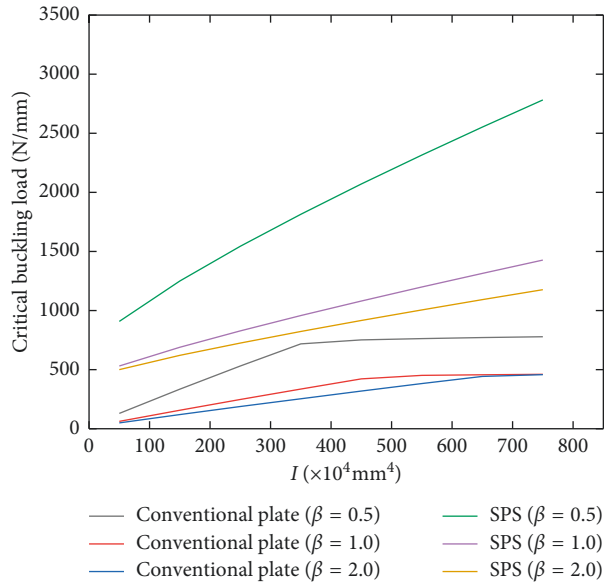

Figure 14: Critical buckling loads in ribbed SPSs and conventional plates with different inertia moments of stiffeners.

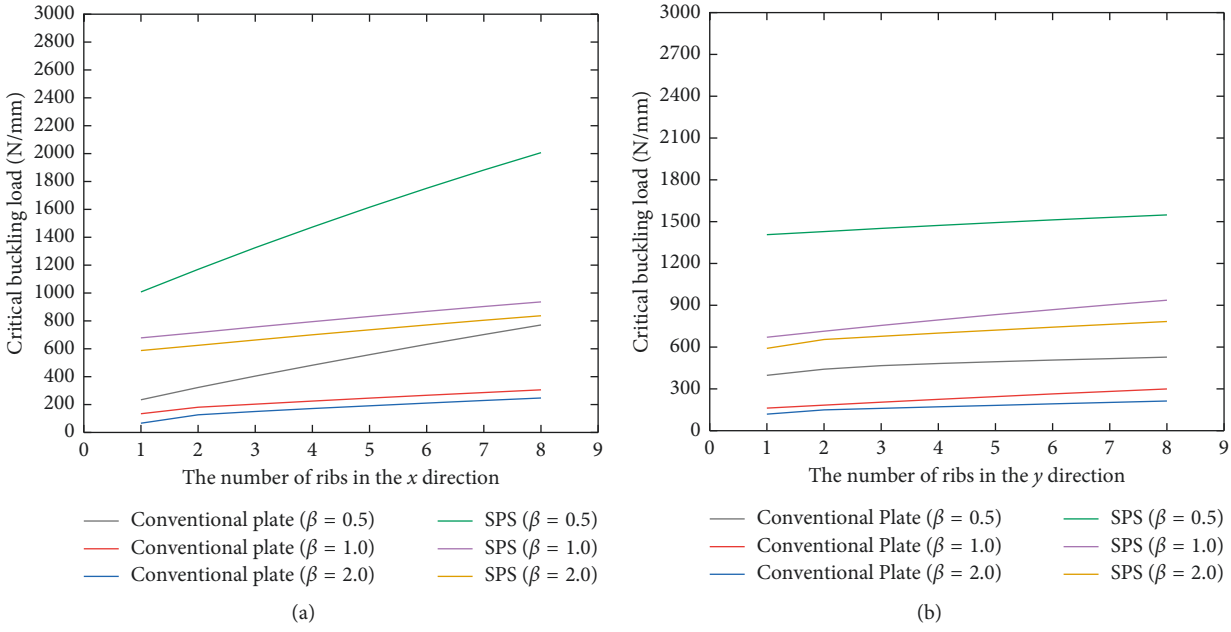

Figure 15: Critical buckling loads in the conventional plates and SPSs with different numbers of ribs: (a) x direction and (b) y direction.

specimens under the available experimental conditions are shown in Figure 16. The faceplates and ribs are constructed from steel with the same thickness (2 mm). The faceplates and reinforcement crossing walls are joined by argon arc welding, forming a closed box. Two holes in the top of the specimen (each of diameter of 20 mm) are formed for filling the polyurethane elastomer. Other holes in the inner walls are manufactured to form a tunnel for pouring the materials (mixed polymer and curing agent) into the full interior of the specimen.

The specimen is prepared as shown in Figure 17. First, the mixed liquid of polymer and curing agent is poured into a closed container. Under air pressure applied by an air compressor, the compound liquid flowed to the opening hole beneath the specimen. Twenty minutes later, the polyurethane elastomer had solidified. The specimen is laid aside for two weeks to fully solidify the elastomer; then, it is tested for its buckling behavior.

Although the stiffeners in the sandwich structure mentioned in the previous calculations have different shapes, the buckling analysis therein is unchanged. To ensure the same constraint conditions in the experiment and the previous analysis, a steel constraining device with V-shaped grooves is designed and installed. This device

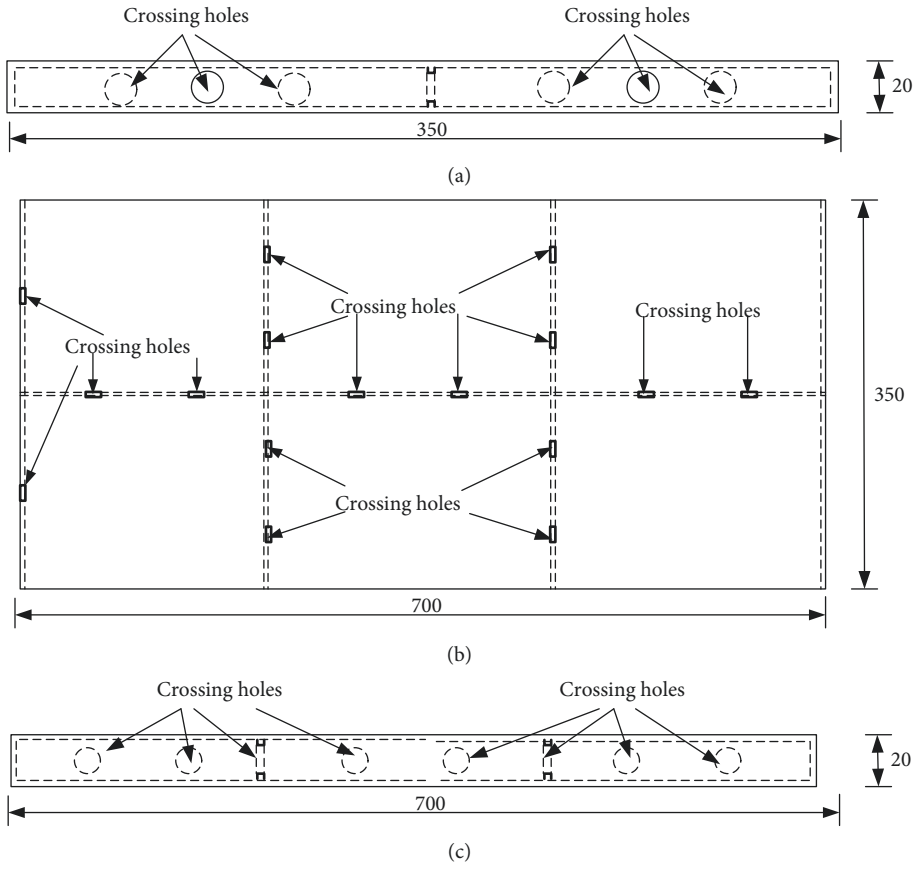

Figure 16: Shape and sizes of the test specimens. (a) Side view of specimen. (b) Top view of specimen. (c) Front view of specimen.

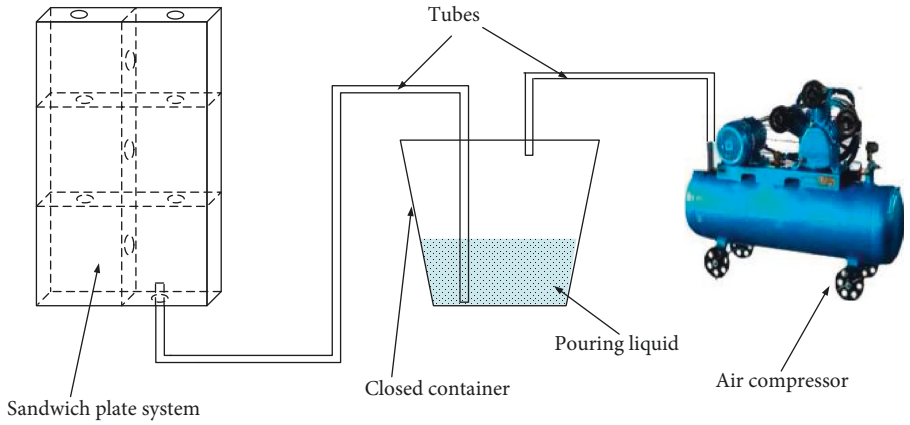

Figure 17: Preparation process of the SPS specimen.

constrained the deflections in the out-of-plane direction only.

4.2. Experimental Results and Discussion. Buckling experiments in a compression test machine are conducted on an SPS model with and without the injected PU elastomer (Figure 18).

The out-of-plane displacements of the SPS experimental model with the stiffeners are constrained by the V-shape grooves installed at all sides, but the boundary deflections in the vertical direction are unrestrained. The pressure is applied by the compression testing machine. The loading speed is 2 mm/min, and the experiments are terminated when the total vertical displacement reached 20 mm. The critical buckling loads obtained in different ways are given in Table 2.

Figure 19 shows the load-displacement curve obtained in the compression experiment. The theoretical and FEM results differed by 5.2% and 3.9%, respectively, from those of

Figure 18: SPS buckling experiment.

Table 2: Critical buckling loads of the test specimens.

Methods	With PU core	Error (with PU core)	Without PU core	Error (no PU core)
Experiment	557.1	N/A	420.3	N/A
Theoretical	585.9	5.2%	544.7	29.6%
FEM	579.0	3.9%	403.4	4.0%

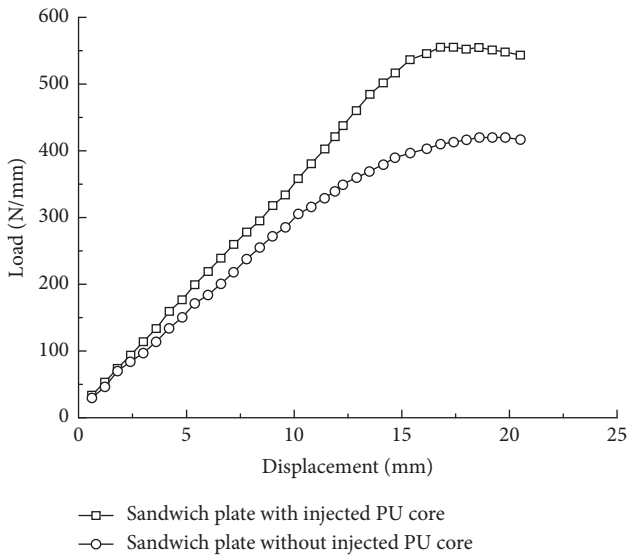

Figure 19: Load-displacement curve obtained in the experiment.

the sandwich plate with a PU core (Table 2 and Figure 19). The difference can be explained by the nonideal boundary constraints in the experiment. In the real case, the boundary constraints are affected by initial bending during welding of the SPS product, which creates a slight gap between the boundary and the fixture device. The results of the sandwich plate without the PU core specimen differed from the FEM and calculation results by almost the same amount (4.0%). However, in the specimen with the PU core, the theoretical and experimental results differed by 29.6%, and the curve change at the position of buckling is less obvious in the experimental specimen. This discrepancy is attributed to local buckling in the corner grids and the assumption of the first-order buckling model, meaning that local buckling appears before the whole structure buckling. In the real case, the PU core can prevent local buckling and raise the buckling strength.

5. Conclusions

A global buckling analysis approach for sandwich plate with stiffening ribs and PU core is discussed here based on theoretical, FEM, and experiments, the following conclusions can be obtained:

(1) The theoretical method present here can forecast the critical global buckling loads and has little error with FEM

(2) SPS can reduce the number of stiffeners and get lager critical buckling loads than conventional steel grillage structure

(3) Inertia moments of ribs influence resistance of buckling failure are limited, because local buckling is appeared before global buckling

(4) The theoretical, FEM, and experiments results show that the existence of PU core in SPS can rise the buckling strength tremendously, about 36.6% in the experiments

Data Availability

The data used to support the findings of this study are included within the article.

Conflicts of Interest

The authors declare that there are no conflicts of interest regarding the publication of this paper.

Acknowledgments

This research was funded by the Natural Science Foundation of Heilongjiang Province (grant number G023017001), the Fundamental Research Funds for the Central Universities (grant number HEUCF180204), the National Natural Science Foundation of China (grant numbers 51409056 and 51678322), and the Taishan Scholar Priority Discipline Talent Group program funded by the Shan Dong Province.

References

[1] D. K. Harris, T. Cousins, T. M. Murray, and E. D. Sotelino, "Field investigation of a sandwich plate system bridge deck," *Journal of Performance of Constructed Facilities*, vol. 22, no. 5, pp. 305–315, 2008.

[2] S. J. Kennedy, J. Bond, D. Braun, P. G. Noble, and J. D. Forsyth, "An innovative "no hot work" approach to hull repair on in-service FPSOs using sandwich plate system overlay," in *Proceedings of Offshore Technology Conference*, Houston, TX, USA, May 2003.

[3] M. Shariyat, "A double-superposition global-local theory for vibration and dynamic buckling analyses of viscoelastic composite/sandwich plates: a complex modulus approach," *Archive of Applied Mechanics*, vol. 81, no. 9, pp. 1253–1268, 2011.

[4] M. Brooking, "The performance, safety and production benefits of SPS structures for double hull tankers," in *Proceedings of RINA Conference on Double Hull Tankers*, London, UK, February 2004.

[5] J. D. Martin, *Sandwich Plate System Bridge Deck Tests*, Virginia Polytechnic Institute and State University, Blacksburg, VA, USA, 2005.

[6] C. Chunlei, L. Yunsheng, and W. Yuanqing, "Behavior analysis of orthotropic steel bridge decks strengthened by SPS," *Journal of Shijiazhuang Tiedao University (Natural Science)*, vol. 3, p. 5, 2010.

[7] D. K. Harris, T. Cousins, E. D. Sotelino, and T. M. Murray, "Flexural lateral load distribution characteristics of sandwich plate system bridges: parametric investigation," *Journal of Bridge Engineering*, vol. 15, no. 6, pp. 684–694, 2010.

[8] G.-q. Feng, G. Li, Z.-h. Liu, H.-l. Niu, and C.-f. Li, "Numerically simulating the sandwich plate system structures," *Journal of Marine Science and Application*, vol. 9, no. 3, pp. 286–291, 2010.

[9] G. Shang, *Ultimate strength study for light weight ship structure*, Ph.D. thesis, Shipbuilding Research Institute of China, Beijing, China, 2011.

[10] K. Liu, Z. L. Wang, Y. C. Zhang, and W. Y. Tang, "Research on the design of hull crashworthiness structure based on sandwich plate system," *Journal of Ship Mechanics*, vol. 18, no. 12, pp. 1505–1514, 2014.

[11] G. Zou, Y. Wu, and Y. Hou, "Study of sandwich plate system in three-point bending considering effect of adhesive," *Materials Research Innovations*, vol. 19, no. 5, pp. 486–489, 2016.

[12] J.-S. Liu and L. Hollaway, "Design optimisation of composite panel structures with stiffening ribs under multiple loading cases," *Computers & Structures*, vol. 78, no. 4, pp. 637–647, 2000.

[13] H.-y. Wang and D.-y. Zhao, "Free vibration analysis of stiffened sandwich plates," *Shipbuilding of China*, vol. 1, p. 14, 2010.

[14] F. Gara, L. Ragni, D. Roia, and L. Dezi, "Experimental tests and numerical modelling of wall sandwich panels," *Engineering Structures*, vol. 37, pp. 193–204, 2012.

[15] M. John and G. Li, "Self-healing of sandwich structures with a grid stiffened shape memory polymer syntactic foam core," *Smart Materials and Structures*, vol. 19, no. 7, article 075013, 2010.

[16] F. Xin and T. Lu, "Analytical modeling of wave propagation in orthogonally rib-stiffened sandwich structures: sound radiation," *Computers & Structures*, vol. 89, no. 5-6, pp. 507–516, 2011.

[17] C. R. Briscoe, S. C. Mantell, T. Okazaki, and J. H. Davidson, "Local shear buckling and bearing strength in web core sandwich panels: model and experimental validation," *Engineering Structures*, vol. 35, pp. 114–119, 2012.

[18] M. D. Goel, V. A. Matsagar, S. Marburg, and A. K. Gupta, "Comparative performance of stiffened sandwich foam panels under impulsive loading," *Journal of Performance of Constructed Facilities*, vol. 27, no. 5, pp. 540–549, 2012.

[19] M. A. Wadee, S. Yiatros, and M. Theofanous, "Comparative studies of localized buckling in sandwich struts with different core bending models," *International Journal of Non-Linear Mechanics*, vol. 45, no. 2, pp. 111–120, 2010.

[20] W. X. Yuan and D. J. Dawe, "Free vibration and stability analysis of stiffened sandwich plates," *Composite Structures*, vol. 63, no. 1, pp. 123–137, 2004.

[21] S. P. Timoshenko and J. M. Gere, *Theory of Elastic Stability*, McGraw-Hill, New York, NY, USA, 1961.

[22] M. Heder, "A simple method to estimate the buckling stress of stiffened sandwich panels," *Composite structures*, vol. 26, no. 1-2, pp. 95–107, 1993.

[23] Q. Zhao, H. Jin, Y. Ding, and P. Chi, "Equivalent laminates model for stiffened panel global buckling analysis," *Acta Materiae Compositae Sinica*, vol. 3, p. 033, 2009.

[24] H. Al-Qablan, "Semi-analytical buckling analysis of stiffened sandwich plates," *Journal of Applied Sciences*, vol. 10, no. 23, pp. 2978–2988, 2010.

[25] C. Amadio and C. Bedon, "Buckling of laminated glass elements in out-of-plane bending," *Engineering Structures*, vol. 32, no. 11, pp. 3780–3788, 2010.

[26] C. Bedon and C. Amadio, "Buckling of flat laminated glass panels under in-plane compression or shear," *Engineering Structures*, vol. 36, pp. 185–197, 2012.

[27] C. Amadio and C. Bedon, "A buckling verification approach for monolithic and laminated glass elements under combined in-plane compression and bending," *Engineering Structures*, vol. 52, pp. 220–229, 2013.

[28] C. Bedon and C. Amadio, "Buckling analysis of simply supported flat glass panels subjected to combined in-plane uniaxial compressive and edgewise shear loads," *Engineering Structures*, vol. 59, pp. 127–140, 2014.

[29] Q. C. Xue, G. P. Zou, Y. Wu, J. Li, and L. Shang, "A comparative study between steel grillage and SPS stiffening plate based on FEA eigen value analysis," *Key Engineering Materials*, vol. 525-526, pp. 337–340, 2013.

[30] Q. C. Xue, G. P. Zou, Y. Wu, H. L. Xiong, and M. Chai, "Calculation for elastic global buckling of sandwich plates with ribs," *Applied Mechanics and Materials*, vol. 188, pp. 25–30, 2012.

[31] N. J. Hoff, "Bending and buckling of rectangular sandwich plates," *Technical Report Archive & Image Library*, vol. 18, no. 2225, p. 330, 1950.